March 16, 2024
www.orbitalscale.com

Calibrating the Pliensbachian-Toarcian transition in Arabia

Moujahed Al-Husseini

Previously Aramco, Saudi Arabia, and GeoArabia, Bahrain
moujaheda@gmail.com

ABSTRACT

The stratigraphic positions of most of the international stage boundaries are not constrained in the Middle East by biostratigraphic control; in turn, this limitation introduces great uncertainties for how to correlate regional transgressive-regressive depositional sequences. This study evaluates alternative criteria for identifying and dating just one example of an unconstrained stage boundary in Arabia, the Pliensbachian-Toarcian boundary. Published carbon-13 isotope ($\delta^{13}C$) records measured across the Pliensbachian-Toarcian carbon-isotope excursion (Pl-T-CIE) are correlated between the Global Stratotype Section and Point (GSSP) in the Penniche section (Portugal), the Mochras borehole (UK), the Chacay Melehue section (Argentina), two boreholes in Kuwait and one section in Oman. The correlation reveals the $\delta^{13}C$ signature spanning the Pl-T-CIE consists of three secular intervals; from base-up: plateau, valley containing the GSSP, and rising limb. The base of the $\delta^{13}C$ plateau correlates to uppermost Pliensbachian global sequence boundary SB JPl8, and further constrains the position of the stage boundary in the overlying $\delta^{13}C$ valley. Another criterion indicates the duration of the interval between SB JPl8 and base Toarcian Stage is c. 500 ka and should consist of five cycle sets tuned by the c. 100 ka short-eccentricity cycle. All these criteria are evident in a Lower Jurassic section in Oman, and consistent with empirical and deterministic estimates for the stage boundary and SB JPl8 at c. 183.7 and c.184.2 Ma.

Key words: Mafraq, Marrat, Saudi Arabia, Kuwait, Oman

1. INTRODUCTION

In the Middle East the precise stratigraphic positions of many Phanerozoic stage boundaries, which are defined and approximately dated in the International Chronostratigraphic Chart of the International Commission on Stratigraphy (ICS. www.stratigraphy.org, Cohen et al., 2013, updated 2023), are not constrained by biostratigraphic control (e.g., Powers, 1968). As a result, it is difficult to date and correlate regional transgressive-regressive (T-R) depositional sequences, sequence boundaries (SB), unconformities, and marine flooding surfaces/intervals (MFS/MFI) between outcrops and the subsurface, across Middle Eastern countries, and to international chronostratigraphic charts (e.g., Le Nindre et al., 1990; Al-Husseini, 1997; Sharland et al., 2001; Haq and Al-Qahtani, 2005; Forbes et al., 2010). The Triassic and Lower Jurassic succession in the Middle East is a typical example in which the positions of international stage boundaries are poorly constrained and regional correlations are highly uncertain (e.g., Powers, 1968; Forbes et al.,

2010; Kadar et al., 2015; Stewart et al., 2016; Issautier et al, 2019; Le Nindre et al., 2023a,b; Crespo de Cabrera et al., 2023).

Although biostratigraphy cannot resolve the positions of many stage boundaries in the Middle East, it can in many sections constrain the stage assignment of formations and members. For example, in outcrop sections in Central Saudi Arabia (Fig. 1, after Scotese, 2023) the middle part of the Marrat Formation yielded Lower Toarcian ammonites (Arkell, 1952; Manivit et al., 1985; Enay and Mangold, 2021), implying the base Toarcian Stage occurs in either the lower part of the formation or in the upper part of the underlying Minjur Sandstone, or possibly at the pre-Marrat unconformity. The present case study considers how to solve this problem using alternative criteria for just this one stage boundary: the base Toarcian Stage in Arabia.

The target for the correlative stratigraphic position of the base Toarcian Stage in the Middle East is represented by its Global Stratotype Section and Point (GSSP; i.e., 'Golden Spike') in the Penniche section in Portugal (Fig. 1) (Bordalo da Rocha et al., 2016), and is summarized in the publication 'Geological Time Scale 2020' – GTS 2020 (Fig. 2, after Hesselbo et al., 2020, in Gradstein et al., 2020). In biostratigraphically complete sections the stage boundary occurs in the Pliensbachian-Toarcian carbon-isotope excursion (Pl-T-CIE) (Fig. 2). Therefore, a possible alternative criterion for identifying the base Toarcian Stage is to correlate its position in Middle Eastern carbon-isotope ($\delta^{13}C$) records to the $\delta^{13}C$ record of the Pl-T-CIE in the Penniche GSSP. Specifically, this study shows the $\delta^{13}C$ record in the GSSP consists of secular patterns with the base Toarcian Stage occurring in a distinct $\delta^{13}C$ valley (Fig. 2).

A second criterion for constraining the position of the base Toarcian Stage in the Middle East may be sought in the sequence architecture spanning the Pl-T-CIE. In particular, uppermost Pliensbachian global sequence boundary SB JPl8 occurs below the base Toarcian Stage in the Spinatum Zone (Haq, 2018; Hesselbo et al., 2020, in Gradstein et al., 2020). It correlates to the base of a $\delta^{13}C$ plateau below the $\delta^{13}C$ valley containing the stage boundary (Ruebsam and Al-Husseini, 2021). Therefore, the $\delta^{13}C$ plateau and valley form a unique $\delta^{13}C$ signature that can be used to recognize the positions of SB JPl8 and the stage boundary (Fig. 2).

In many studies a glacio-eustatic fall is interpreted in the latest Pliensbachian (e.g., Brandt, 1986; Boulila et al., 2014; Krencker et al., 2019; Ruebsam et al., 2019; Nordt et al., 2022; Chang et al., 2023), implying SB JPl8 represents a glaciation that may have been orbitally forced and that its age may be approximately predicted by the deterministic orbital scale of glacio-eustasy (Matthews and Frohlich, 2002; Matthews and Al-Husseini, 2010; see Supplementary Information, abbreviated S.I.). The scale predicts SB JPl8 occurs at the minimum eccentricity at the base of 405-ka Straton 455 (13B-6) at 184.24 Ma, consistent with empirical estimates of 184.3 Ma (Haq, 2018), and between 184.4 and 184.1 Ma (Ruebsam and Al-Husseini, 2021). The scale estimates the stage boundary at c. 183.7 Ma in Straton 454 (13B-7) (Ruebsam and Al-Husseini, 2020, 2021), consistent with the radiometric estimates of 183.8 ± 0.4 Ma (Ruhl et al., 2016), 183.73 +0.35/-0.50 Ma (Al-Suwaidi et al., 2022) and 183.7 Ma in both the GTS 2016 (Ogg et al., 2016) and the Astronomical Time Scale (ATS, Huang, 2018). These estimates provide a third criterion that indicates the duration of the interval between SB JPl8 (base $\delta^{13}C$ plateau) and the stage boundary (in the $\delta^{13}C$ valley) is c. 500 ka, and should consist of five stratigraphic cycles tuned at c. 100 ka.

In the case of limited biostratigraphic constraints these three criteria are considered alternative and/or supporting constraints for identifying and dating the correlative stratigraphic position of the base Toarcian Stage in the Middle East. The study is a synthesis of published data, methods and interpretations in the literature; as such a 'Data and Methods' section is not included in this article. Instead, the relevant published data and analyses are discussed in this case study for the Penniche GSSP section noted above (Fig. 2, Bordalo da Rocha et al., 2016), the Mochras borehole (Cardigan Bay Basin, UK, Copestake and Johnson, 2013; Percival et al., 2015; Xu et al., 2018; Storm et al., 2020; Ruebsam and Al-Husseini, 2020, 2021; Ruebsam et al., 2020), the Chacay Melehue (CM) section in Argentina (Al-Suwaidi et al., 2022), two boreholes in Kuwait (Crespo de Cabrera et al., 2023; De Keyser et al., 2024, in review) and the type section of the Mafraq Formation in Oman (Bendias and Aigner, 2015) (Fig. 1).

2. POSITION OF THE BASE TOARCIAN STAGE IN THE PL-T-CIE

2.1 Reference section

The Pl-T-CIE and the younger Early Toarcian T-CIE are documented by $\delta^{13}C$ organic and $\delta^{13}C$ carbonate records in numerous sections worldwide (Ruebsam and Al-Husseini, 2020, 2021, and references therein). Many sections contain unconformities and condensed intervals rendering it difficult to consistently identify the $\delta^{13}C$ valley containing the stage boundary and other $\delta^{13}C$ correlative patterns. However, based on a review of $\delta^{13}C$ records from several presumably biostratigraphically complete sections, the $\delta^{13}C$ records generally consist of key secular patterns (falling and rising limbs, valleys and plateaus), and distinct cycles that can be used to construct a representative $\delta^{13}C$ reference section calibrated by ammonite zones (Fig. 3, Table S1, Ruebsam and Al-Husseini, 2020, 2021; Ruebsam et al., 2020).

2.2 Mochras Borehole

The $\delta^{13}C$ record in the Mochras borehole closely resembles that in the reference section and was therefore chosen for cyclostratigraphic analyses and age dating (Fig. 3, Storm et al., 2020; Ruebsam and Al-Husseini, 2020, 2021; Ruebsam et al., 2020). It contains a high-resolution Pliensbachian-Toarcian $\delta^{13}C$ record calibrated by the Spinatum, Tenuicostatum, Serpentinum and Bifrons ammonite zones (Storm et al., 2020, and references therein). In this borehole the boundaries of the $\delta^{13}C$ secular patterns and ammonite zones are picked to an accuracy of better than one meter (Fig. 3, Table S1).

In the Mochras borehole the base Toarcian Stage occurs in the $\delta^{13}C$ valley, above a plateau and below a rising limb (Fig. 3). These secular patterns closely resemble those in the $\delta^{13}C$ records in the Penniche GSSP and the CM sections; moreover, in all three sections the $\delta^{13}C$ plateau consists of upper and lower plateaus (Fig. 4). However, whereas in the Penniche and Mochras sections the stage boundary occurs in the $\delta^{13}C$ valley, in the CM section it occurs in the upper $\delta^{13}C$ plateau (Fig. 4).

In the CM section Al-Suwaidi et al. (2022) chose the position of the stage boundary in the upper $\delta^{13}C$ plateau and correlated it to the upper $\delta^{13}C$ plateau in the Mochras borehole in their figure 5 (Fig. S1). As a result, the biostratigraphic stage boundary in the Mochras borehole was shifted downwards by c. 3 m (from 863 to 866 m). Shifting the boundary from the $\delta^{13}C$ valley to the plateau,

if also applied to the Penniche section, would shift the stage boundary from c. -0.30 to -0.75 m to below the FO of *D. (Eodactylites)* cf. simplex (Fig. 4), and alter the definition of the GSSP.

2.3 Significance of shifting the FO

The different positions of the FO of *D. (Eodactylites)* cf. simplex relative to the $\delta^{13}C$ secular patterns in the Penniche GSSP and CM sections suggests this biostratigraphic event is not isochronous. This hypothesis seems likely when considering the paleogeography of the Early Jurassic (Fig. 1). Whereas the CM section was situated in western South America in the eastern Panthalassic realm, the Penniche and Mochras sections were located in NW Europe in the westernmost Neo-Tethys realm. The two realms were in communication across the entire Panthalassic and Neo-Tethys oceans spanning a latitudinal distance of c. 24,000 km, or possibly via the narrow and restricted c. 6,000 km-long Hispanic Corridor (Fig. 1). It seems highly improbable that *D. (Eodactylites)* cf. simplex first appeared across such vast distances at the same time. On the other hand, the Pl-T-CIE represents a global event associated with the Karoo-Ferrar Large Igneous Province (K-F-LIP) in southern Gondwana (Palfy and Smith, 2000; Xu et al., 2018; Al-Suwaidi et al., 2022). The LIP caused essentially synchronous atmospheric and oceanic perturbations to the carbon cycle, as expressed in globally correlative $\delta^{13}C$ records.

2.4 Base Toarcian Stage in Kuwait

The position for the FO of *D. (Eodactylites)* cf. simplex in different $\delta^{13}C$ intervals raises a fundamental question: should the stage boundary in the Middle East be chosen in the $\delta^{13}C$ valley or in the upper plateau? The choice is illustrated in deep boreholes in Kuwait where biostratigraphy indicates the Pliensbachian-Toarcian transition spans the boundary between the Lower Marrat (LM) and Middle Marrat (MM) members (Fig 4) (Crespo de Cabrera et al., 2023). This transition contains $\delta^{13}C$ records in boreholes JJ and X, which closely resemble the plateau, valley and rising limb segments in the Pl-T-CIE in the Penniche, Mochras and CM sections (De Keyser et al., 2024, in review, Fig. 4). Based on paleogeographic considerations and the correlation of the $\delta^{13}C$ records, the correlative position of the stage boundary in the GSSP is chosen in the $\delta^{13}C$ valley at c. 15,773 ft in the JJ borehole and c. 15,708 ft in the XX borehole (Fig. 4).

3. POSITION OF PLIENSBACHIAN SEQUENCE BOUNDARY SB JPL8

3.1 Global SB JPl8

Global SB JPl8 is the youngest Pliensbachian sequence boundary and occurs in the Spinatum Zone (Haq, 2018). In the Mochras borehole Ruebsam and Al-Husseini (2021, their figure 4) positioned SB JPl8 at the base of the lower $\delta^{13}C$ plateau (Fig. 3), and correlated the base plateau to an unconformity in the Sancerre section in France (Peti et al., 2017), a possible unconformity in the Shandelah borehole (North German Basin, van de Schootbrugge et al., 2018), and a major erosion surface characterized by incised channels with depths of 45 to 75 m in the Spinatum Zone in the North Sea (Marjanac and Steel, 1997). This unconformity is coincident with global cooling and interpreted as a glacio-eustatic fall; it is expressed as a biostratigraphic hiatus informally named the 'spinatum chemostratigraphic black hole' (Fig. 3, Ruebsam and Al-Husseini, 2021) or 'SBH-1' in Ruebsam and Al-Husseini (2020).

In the Penniche section, Bordalo da Rocha et al. (2016, their figure 2) interpreted a major regression in late Pliensbachian ending with an SB at the base Toarcian Stage, followed by an earliest Toarcian

'fast transgression' with the MFI positioned one meter above the boundary. Nordt et al. (2022, their figure 2) also positioned the global SB at the stage boundary at 182.7 Ma (instead of 183.7 Ma). In the global framework, however, the stage boundary is not interpreted as an SB (e.g., Haq, 2018; Ruebsam and Al-Husseini, 2021). Indeed in GTS 2020, Hesselbo et al. (2020, their figure 26.10 on p. 979 and 980, in Gradstein et al., 2020) depict a late Pliensbachian T-R megacycle that ends at SB JPl8 at c. 184.8 Ma in the Spinatum Zone, and they assign the entire Toarcian Stage within just one T-R megacycle between SB JPl8 and SB Aa2 at c. 173 Ma in the Aalenian Stage. These two megacycles, as shown in GTS 2020, support positioning SB JPl8 in the latest Pliensbachian Spinatum Zone rather than at the base Toarcian Stage.

3.2 SB JPl8 in Kuwait

The sequence architecture in the Pliensbachian-Toarcian transition in Kuwait is interpreted in cores extracted from deep boreholes by Kuwait Oil Company and summarized below from Crespo de Cabrera et al. (2023) and De Keyser et al. (2024, in review). The transition occurs in a T-R sequence denoted 'J10' in Kuwait. The lower boundary of 'Sequence J10' is denoted 'SB J10' and corresponds to an unconformity in cores extracted from four boreholes, and occurs at c. 15,831 ft at the base of a thin shale bed (Fig. 4). Above the shale bed massive anhydrites (occasionally interbedded with dolomitized microbial laminite boundstones) are interpreted as the lowstand systems tract (LST) of 'Sequence J10'. The LST deposits are overlain by interbedded dolomitic and anhydritic mudstones with common intraclasts interpreted as the transgressive systems tract (TST) of 'Sequence J10'. The TST interval is overlain by an interval of limestones interpreted as the highstand systems tract (HST) with 'MFS J10' positioned between the TST and HST tracts, and coincident with the base of the $\delta^{13}C$ rising limb. 'MFS J10' in Kuwait is not to be confused with MFS J10 as defined by other authors (e.g., Sharland et al., 2001; Farouk et al., 2018; Al-Mojel et al., 2020).

'SB J10' is a regional sequence boundary at the base of T-R 'Sequence J10' and is correlated with gamma-ray logs in numerous boreholes across Kuwait (see figure 22 in Crespo de Cabrera et al., 2023). In borehole JJ, 'SB J10' occurs at c. 15,831 ft and approximately 58 feet (c. 19 m) below the position of the base Toarcian Stage at c. 15,773 ft in the $\delta^{13}C$ valley (Fig. 4). 'Sequence J10' evolved from LST to TST and HST and does not contain any intermediate unconformities, implying 'SB J10' is the youngest sequence boundary in uppermost Pliensbachian and correlates to global SB JPl8 below the stage boundary.

3.3 Pre-Marrat unconformity in Saudi Arabia

As noted in the introduction, the stratigraphic position of the base Toarcian Stage in Saudi Arabia is not constrained by biostratigraphy. The Marrat Formation was deposited as a major regional transgression across Arabia on the pre-Marrat unconformity. The formation overlies the Minjur Sandstone dated as late Pliensbachian and older, as well as other yet-older formations (Powers, 1968; Stewart et al., 2016; Issautier et al., 2019). In the outcrop belt in Central Saudi Arabia the middle part of the Marrat Formation yielded Lower Toarcian ammonites in several sections (Arkell, 1952; Enay and Mangold, 2022). By stratigraphic position and regional extent the pre-Marrat unconformity is the most likely correlative for global SB JPl8, implying the base Toarcian Stage occurs in the lower part of the Marrat Formation. This hypothesis can be tested by measuring $\delta^{13}C$ values across the lower part of the Marrat Formation to determine if it contains the signature of the Pl-T-CIE.

4. AGE ESTIMATES OF SB JPl8 AND THE BASE TOARCIAN STAGE

Estimating the ages of SB JPl8 and the base Toarcian Stage is important in order to determine the duration of the intervening interval and their relationships to global events (e.g., Karoo-Ferrar LIP, climate changes, glacio-eustasy). In the GTS 2016 Ogg et al. (2016) estimated the stage boundary at 183.7 Ma, and Haq (2018) adopted this age to estimate SB JPl8 at 184.3 Ma. However, in the GTS 2020 Hesselbo et al. (2020, in Gradstein et al., 2020) estimated both surfaces as 500–600 ka older at 184.2 and 184.8 Ma. In the website version of the International Chronostratigraphic Chart v. 2023/9 of the ICS (Cohen et al., 2013, updated 2023) the stage boundary is estimated at 184.2 ± 0.3 Ma. These estimates can be refined based on more recent radiometric data.

In the CM section Al-Suwaidi et al. (2022) obtained a radiometric estimate of 184.10 ± 0.54 Ma within the lower $\delta^{13}C$ plateau (Fig. 4), and the mean estimate is consistent with the combined radiometric-cyclostratigraphic estimate for the base of the lower $\delta^{13}C$ plateau between 184.4 and 184.1 Ma (Ruebsam and Al-Husseini, 2021). These empirical estimates indicate the base of the lower $\delta^{13}C$ plateau has a mean age between c. 184.1 and 184.4 Ma, more consistent with the estimate for SB JPl8 of 184.3 Ma (Haq, 2018), rather than 184.8 Ma (Hesselbo et al., 2020, in Gradstein et al., 2020).

Huang (2018) adopted the age estimate for the base Toarcian Stage at 183.7 Ma (Ogg et al., 2016), and positioned it at the maximum eccentricity value of long-eccentricity cycle E454 in the 405-ka metronome of the Astronomical Time Scale (ATS; Laskar et al., 2004; Hinnov, 2018). A similar result can be obtained by estimating the age of SB JPl8 based on a model of eccentricity-forcing of glacio-eustasy (Matthews and Frohlich, 2002; Matthews and Al-Husseini, 2010, S.I.). This independent approach predicts SB JPl8 occurs at the minimum eccentricity at the base of 405-ka Straton 455 (13B-6) at c. 184.24 Ma and the stage boundary at the maximum eccentricity of E454 at 183.65 Ma (Fig. 4, S.I.) (Ruebsam and Al-Husseini, 2020, 2021; Ruebsam et al., 2020).

5. STAGE BOUNDARY AND SB JPL8 IN OMAN

The Lower Jurassic Mafraq Formation in Oman is dated by contradictory biostratigraphic interpretations, and therefore provides a suitable target to test the application of alternative criteria. The type section of the Mafraq Formation is defined in Wadi Sahtan (Figs. 1 and 5, Bendias and Aigner, 2015), and its reference section is defined c. 200 km farther west in the Lekhwair-70 borehole (Forbes et al., 2010). In both sections the formation is unconformably overlain by the Bajocian Dhruma Formation, and in Wadi Sahtan it unconformably overlies Triassic sediments (Forbes et al., 2010; Bendias and Aigner, 2015; P. Nederloff, pers. comm. 2021). The type and reference sections of the formation are dated by the same micropaleontological and palynological zones of Petroleum Development Oman (PDO), but the zones are assigned to completely different Lower and Middle Jurassic stages.

In the Wadi Sahtan section, the Lithiotis fauna provides an important clue towards resolving the approximate age of the formation. The Lithiotis Limestone interval, between 82 and 33 m (Fig. 5), constrains the age of this interval to Pliensbachian-early Toarcian. The extinction of the Lithiotis fauna is a regional event across the southern Neo-Tethys realm and occurs below the Toarcian T-CIE (Baeza-Carratala et al., 2017; Posenato et al., 2018; Han et al., 2022). The extinction level at 33 m implies the uppermost negative $\delta^{13}C$ excursions in the Mafraq Formation corresponds to the

lower part of the Early Toarcian T-CIE, and the $\delta^{13}C$ excursion, between c. 112 and 63 m, represents the Pl-T-CIE (Fig. 5). Importantly, the Pl-T-CIE interval contains the same $\delta^{13}C$ secular patterns seen in other Neo-Tethys sections; from base-up: lower and upper plateaus, valley, and rising limb.

The sequence architecture of the Mafraq Formation is interpreted by 23 cycle sets (CS), grouped into six high-frequency sequences (HFS) in the Lower Mafraq T-R Sequence (LM HFS-1 to LM HFS-6), and two HFS's in the Upper Mafraq T-R Sequence (UM HFS-1 and UM HFS-2) (Fig. 5, Bendias and Aigner, 2015). The base Toarcian Stage GSSP occurs in the lower part of the $\delta^{13}C$ valley, corresponding to CS-9, and SB JPl8 corresponds to the base of the lower $\delta^{13}C$ plateau at base CS-13 (Figs. 3 to 5). The average duration of the cycle sets is unknown, but assuming they are tuned by the short-eccentricity c. 100-ka cycle then they would provide a floating chronometer. Based on this assumption, the two plateaus (CS-13 to CS-10) represent c. 400 ka, and the lower valley (CS-9) c. 100 ka totaling c. 500 ka. The difference of 500 ka between the estimates for SB JPl8 (c. 184.2 Ma) and the stage boundary (c. 183.7 Ma) is consistent with the assumption the five cycle sets (CS-13 to CS-9) are tuned at c. 100 ka and together represent c. 500 ka.

Cycle set CS-8 contains the MFS of the Lower Mafraq T-R Sequence in the lower part of the $\delta^{13}C$ valley. In contrast, in the Penniche and Kuwait sections the MFS occurs at the top of the $\delta^{13}C$ valley corresponding CS-7 in Wadi Sahtan. The different stratigraphic positions for the MFS relative to the $\delta^{13}C$ valley (lower part or at its top) suggests the change from TST to HST may vary from locality to locality.

The interval CS-7 to CS-1 represents c. 700 ka but resolving it into the rising limb and T-CIE falling limb as characterized in the reference section is unclear (Fig. 3). The switch from rising to falling limbs may occur in CS-5 at the base of UM HFS-1 where early Toarcian SB JTo1 and the tenuicostatum chemostratigraphi hiatus occurs in the reference section (Fig. 3).

6. SUMMARY AND CONCLUSIONS

Three independent criteria are evaluated in this case study to constrain the position and age of the base Toarcian Stage in the Middle East and specifically in Arabia. The criteria are guided by broad biostratigraphic interpretations in the target stratigraphic interval and the $\delta^{13}C$ data sets were not specifically acquired to identify the base Toarcian Stage. Therefore, acquiring additional $\delta^{13}C$ data sets and relating them to sequence architectures in other Toarcian sections or geologic intervals may better constrain or possibly resolve international stage boundaries in the Middle East.

The first constraint identified the stratigraphic position of the stage boundary in the Penniche GSSP section (Portugal) in a distinct $\delta^{13}C$ valley in the Pliensbachian-Toarcian carbon-isotope excursion (Pl-T-CIE). The $\delta^{13}C$ valley also occurs in the Mochras borehole (UK), Chacay Melehue section (Argentina), two boreholes in Kuwait and a section in Oman, thus providing a correlative $\delta^{13}C$ position for the stage boundary.

The second criterion correlated uppermost Pliensbachian global sequence boundary SB JPl8 to the base of the $\delta^{13}C$ lower plateau in the Pl-T-CIE in the Mochras section and to an unconformity in Kuwait and in sections in other realms. In Kuwait the unconformity marks the base of regional T-R 'Sequence J10' that contains the $\delta^{13}C$ valley and therefore further confirms the chosen position

for the base Toarcian Stage. Sequence boundary SB JPl8 marks the base of a global mega-scale T-R sequence and most likely correlates to the regional pre-Marrat unconformity in Saudi Arabia, implying the base Toarcian Stage occurs in the lower part of the Marrat Formation.

Based on radiometric dating and the predictions of the deterministic orbital scale of glacio-eustasy, the positions of base Toarcian Stage in the $\delta^{13}C$ valley and SB JPl8 at the base of the $\delta^{13}C$ plateau are estimated at c. 183.7 and 184.2 Ma. Confirming that the intervening interval represents c. 500 ka provides a third criterion. In the Mafraq Formation in the Wadi Sahtan section in Oman the base plateau to lower part of the valley in the $\delta^{13}C$ record consists of five cycle sets most likely tuned at c. 100 ka.

Comment

This study is an update to two preliminary reports on the presumed Toarcian $\delta^{13}C$ data in the Mafraq Formation in Oman and the Marrat Formation in Kuwait (Al-Husseini, 2022a, b). The two open-access reports were posted in www.orbitalscale.com and ResearchGate in early 2022 in order to highlight how $\delta^{13}C$ data sets could be used to establish regional correlations between Arabia and Europe. However, the reports were based on incomplete data sets leading to incorrect interpretations and conclusions. Nonetheless, the two reports achieved an important objective when in February 2024 Kuwait Oil Company and the Kuwait Ministry of Oil released for publication a major study on the carbon-isotope stratigraphy in Kuwait by De Keyser et al. (2024) currently in review.

Acknowledgements

The author thanks Arnold Egdane for designing the manuscript.

References

Al-Husseini, M.I. 1997. Jurassic sequence stratigraphy of the western and southern Arabian Gulf. GeoArabia, v. 2, no. 4, p. 361-382.

Al-Husseini, M.I. May 10, 2022a. Late Pliensbachian-early Toarcian Mafraq Formation of Oman, www.orbitalscale.com. 14 p.

Al-Husseini, M.I. June 1, 2022b. Toarcian carbon-isotope stratigraphy and ammonite zones in Kuwait. www.orbitalscale.com. 20 p.

Al-Mojel., A., Razin, P., Le Nindre Y.-M., and Dera, G., 2020. Shallow-marine depositional sequences in a transgressive mixed siliciclastic-carbonate system: the Early Jurassic Marrat Formation from Central Saudi Arabia. Journal of African Earth Sciences. 167, 103429.

Al-Suwaidi, A., Ruhl, M., Jenkyns, H. C., et al, 2022. New age constraints on the Lower Jurassic Pliensbachian-Toarcian boundary at Chacay Melehue (Neuquen Basin). Argentina. Scientific Reports 12, 4975.

Arkell, W.J., 1952. Jurassic ammonites from Jebel Tuwaiq, central Arabia. Philosophical Transactions of the Royal Society of London B 236, 241–313.

Baeza-Carratala, J.F., Joral, F.G., Goy, A., and Tent-Manclús, J.E., 2017. Arab- Madagascan brachiopod dispersal along the North-Gondwana paleomargin towards the Western Tethys Ocean during the Early Toarcian (Jurassic), Palaeogeogr. Palaeoclimatol. Palaeoecol. 490, 252–268.

Bendias, D., and Aigner, T., 2015. Facies, sequence stratigraphy, reservoir and seal potential of the Mafraq Formation, Sultanate of Oman: An integrated outcrop analogue study. GeoArabia, 2015, v. 20, no. 3, p. 17-94**.**

Boulila, S., Galbrun, B., Huret, E., Hinnov, L.A., Rouget, I., Gardin, S., and Bartolini, A., 2014. Astronomical calibration of the Toarcian Stage: Implications for sequence stratigraphy and duration of the early Toarcian OAE. Earth Planet. Sci. Lett. 386, 98–111.

Bordalo da Rocha, R., Mattioli, E. Duarte, L.V., Pittet, B., lmi, S., Mouterde, R., Cabral, M.C., Comas-Rengifo, M.J., Gómez, J.J.,, Goy, A., Hesselbo, S.P., Jenkyns. H.C.., Littler. K., Mailliot, S., Veiga de Oliveira. L.C., Osete M.L., Perilli, N., Pinto, S., Ruget, C. and Suan, G., 2016. Base of the Toarcian Stage of the Lower Jurassic defined by the Global Boundary Stratotype Section and Point (GSSP) at the Peniche section (Portugal). Episodes Vol. 39, no. 3, 460-481.

Brandt, K., 1986. Glacioeustatic cycles in the Early Jurassic? Neues Jahrbuch für Geologie und Paläontologie, 5, 257–274.

Chang, C.Y., Kinney, S.T., Fang, Y, Sha, J. and Olsen, P. 2023. Quantitative evidence for Arctic continental freezing in a high-CO2 world: Junggar Basin, NW China. In: Sha, J., Slater, S. M., Vajda, V., Olsen, P. E. and Zhang, H. (eds) The Triassic and Jurassic of the Junggar Basin, China: Advances in Palaeontology and Environments. Geological Society, London, Special Publications, 538, https://doi.org/10.1144/SP538-2023-1.

Cohen, K.M., Finney, S.C., Gibbard, P.L. and Fan, J.-X. (2013; updated). The ICS International Chronostratigraphic Chart. Episodes 36: 199-204. http://www.stratigraphy.org/ICSchart/ChronostratChart2023-09.pdf

Copestake, P. and Johnson, B., 2013. Lower Jurassic Foraminifera from the Llanbedr (Mochras Farm) Borehole, North Wales, UK. Monogr. Palaeontogr. Soc. 167, 1-403.

Crespo de Cabrera, S., De Keyser, T., Al-Sahlan, G., Al-Wazzan, H.A. and Kadar, A.P. 2023, Biostratigraphy and sequence stratigraphy of the Minjur and Marrat Formations (Upper Triassic to Middle Jurassic) in Kuwait . Stratigraphy, vol. 20, no. 3, 155–224.

De Keyser, T., Ruebsam, W., Al-Husseini, M., Crespo de Cabrera, S., Al-Sahlan, G., and Swart, P., 2024 (in review). Carbon-isotope stratigraphy of the Toarcian in Kuwait.

Enay R. and Mangold, Ch., 2021. Jurassic ammonites from Central Saudi. Arabia (Jebel Tuwaiq and adjacent areas). Revue de Paléobiologie, 40(1), 197 p.

Farouk, S., Al-Kahtany, K., El-Sorogy, A., and Abd El-Motaal, E., 2018. High-frequency cycles and sequence stratigraphy of the lower Jurassic Marrat Formation, centralSaudi Arabia. Marine and Petroleum Geology 98, 369–383.

Forbes, G., Jansen, H., and Schreurs, J., 2010. Lexicon of Oman Subsurface Stratigraphy: Reference Guide to the Stratigraphy of Oman's Hydrocarbon Basins. GeoArabia Special Publication 5, Gulf PetroLink, Bahrain, 371 p.

Gradstein, F.M., Ogg, J.G., Schmitz, M.D., and Ogg, G.M. (Eds.), Geologic Time Scale 2020, Elsevier Inc.

Han, Z., Hu, X., Hu, Z., Jenkyns, H. C., and Su, T., 2022. Geochemical evidence from the Kioto Carbonate Platform (Tibet) reveals enhanced terrigenous input and deoxygenation during the early Toarcian. Global and Planetary Change 215, 103887.

Haq, B.U., 2018. Jurassic sea level variations: a reappraisal. Geol. Soc. America, GSA Today, 1, soi: 10.1130/GSATG359A.1

Haq, B.U. and Al-Qahtani, A.M., 2005. Phanerozoic cycles of sea-level change on the Arabian Platform. GeoArabia 10(2), 127–160.

Hesselbo, S.P., Ogg, J.G., Ruhl, M., Hinnov, C., and Huang, C., 2020. Chapter 26, The Jurassic Period.

Geologic Time Scale 2020, v. 2, 965–1021. Elsevier.

Hinnov, L., 2018. Cyclostratigraphy and Astrochronology in 2018 In: Montenari, M. (Ed.), Stratigraphy and Timescales. vol. 3. 1–80, Elsevier Inc,

Huang, C., 2018. Astronomical time scale for the Mesozoic. In: Montenari, M. (Ed.), Stratigraphy and Timescales. vol. 3. p. 81–150. Elsevier Inc,

Issautier, B., Le Nindre Y.-M., Hooker, N. P., Reid C., Memesh A., and Dini S.. 2019. Depositional environments, age, and sequence stratigraphy of the Minjur Formation in outcrop and near subsurface - Central Saudi Arabia. In R. Steel, H. Al-Anzi, R. Rahmani and O. Soliman (Eds.), Siliciclastic Reservoirs of the Arabian Plate. AAPG Memoir 116, 141–183.

Kadar, A.P., De Keyser, T., Neog, N. and Karam, K. (with contributions from Le Nindre, Y. M. and Davies, R. B.), 2015. Calcareous nannofossil zonation and sequence stratigraphy of the Jurassic System, onshore Kuwait. *GeoArabia*, 20 (4): 125–180.

Krencker, F.-N., Lindström, S., and Bodin, S., 2019. A major sea-level drop briefly precedes the Toarcian oceanic anoxic event. Implication for early Jurassic climate and carbon cycle. Sci. Rep. 9, 12518.

Laskar, J., Robutel, P., Joutel, F., Gastineau, M., Correia, A.C.M., and Levrard, B. 2004. A long-term numerical solution for the insolution quantities of the Earth. Astron. Astrophys. 428, 261–285.

Le Nindre, Y.-M., Manivit, J., and Vaslet, D., 1990. Stratigraphie séquentielle du Jurassique et du Crétacé en Arabie Saoudite. Bulletin, Société géologique de France, Paris, sér. 8, v. VI, p. 1025-1034.

Le Nindre, Y.-M., Vaslet, D., Vrielynck, B., Krystyn, L., Manivit, J., Memesh, A., and Davies, R.B., 2023a. The Middle to Late Triassic of Central Saudi Arabia with emphasis on the Jilh Formation. Part I: lithostratigraphy, facies and paleoenvironments, palaeontology and biostratigraphic age calibration from outcrop studies. In Comptes Rendus Geoscience Special Publication 'Tribute to Jean Dercourt' (Eds F. Baudin, E. Calais and F. Chabaux). https://doi.org/10.5802/crgeos.217

Le Nindre, Y.-M., Davies, R.B. Issautier, B. Krystyn, L., Vaslet, D., Vrielynck, B., and Memesh, A., 2023b, The Middle to Late Triassic of Central Saudi Arabia with emphasis on the Jilh Formation. Part II: sequence stratigraphy, depositional and structural history, correlations and paleogeography. In Comptes Rendus Geoscience Special Publication 'Tribute to Jean Dercourt' (Eds F. Baudin, E. Calais and F. Chabaux). https://doi.org/10.5802/crgeos.227

Littler, K., Hesselbo, S.P., and Jenkyns, H.C., 2010. A carbon-isotope perturbation at the Pliensbachian-Toarcian boundary: evidence from the Lias Group, NE England. Geological Magazine 147 (2), 181–192.

Manivit, J., Pellaton, C., Vaslet, D., Le Nindre, Y.-M., Brosse, J.-M., Breton, J.-P., Fourniguet, J., and Prevot, J.-C., 1985. Explanatory notes to the geologic map of the Darmā Quadrangle, Kingdom of Saudi Arabia. Geoscience map GM-101C, scale 1:250,000, sheet 24H. Deputy Ministry for Mineral Resources, Ministry of Petroleum and Mineral Resources, Kingdom of Saudi Arabia. 33 p.

Marjanac, T. and Steel, R.J., 1997. Dunlin Group Sequence Stratigraphy in the northern North Sea: A Model for Cook Sandstone Deposition. AAPG Bulletin 81, 276–292.

Matthews, R.K., and Frohlich, C., 2002. Maximum flooding surface and sequence boundaries: Comparisons between observation and orbital forcing in the Cretaceous and Jurassic (65-190 Ma). GeoArabia 7(3), 503–538.

Matthews, R.K., and Al-Husseini, M.I., 2010. Orbital-forcing glacio-eustasy: a sequence-stratigraphic time scale. GeoArabia 15 (3), 155–167.

Nordt, L., Breecker, D., and Wihte, J. (2022). Jurassic greenhouse ice-sheet fluctuations sensitive to atmospheric CO2 dynamics. Nat. Geosci. 15, 54–59.

Ogg, J., Ogg, G., and Gradstein, F., 2016. A Concise Geologic TimeScale 2016. Elsevier Inc,.

Palfy, J., and Smith, P.L., 2000. Synchrony between early Jurassic extinction, oceanic anoxic event, and the Karoo-Ferrar flood basalt volcanism. Geology 28, 747–750.

Percival, L.M.E. et al. 2015. Globally enhanced mercury deposition during the end-Pliensbachian extinction and Toarcian OAE: A link to the Karoo-Ferrar Large Igneous Province. Earth Planet. Sci. Lett. 428, 267–280.

Peti, L., Thibault, N., Clémence, M.E., Korte, C., Dommergues, J.L., Bougeault, C., Pellenard, P., Jelby, M.E., and Ullmann, C.V., 2017. Sinemurian–Pliensbachian calcareous nannofossil biostratigraphy and organic carbon isotope stratigraphy in the Paris Basin: calibration to the ammonite biozonation of NW Europe. Palaeogeogr. Palaeoclimatol. Palaeoecol. 468, 142–161.

Posenato, R., Bassi, D., Trecalli, A., and Parente, M., 2018. Taphonomy and evolution of Lower Jurassic lithiotid bivalve accumulations in the Apennine Carbonate Platform (southern Italy). Palaeogeography, Palaeoclimatology, Palaeoecology, v. 489, p. 261–271.

Powers, R.W., 1968. Lexique stratigraphique international. Volume III, Asie, Fas. 10 b1, Saudi Arabia. Centre Nationale de la Recherche Scientifique, Paris, 177 p.

Ruebsam, W. and Al-Husseini, M.I, 2020. Calibrating the Early Toarcian (Early Jurassic) with stratigraphic black holes (SBH). Gondwana Research 82, 317–336.

Ruebsam, W. and Al-Husseini, M.I., 2021. Orbitally synchronized late Pliensbachian– early Toarcian glacio-eustatic and carbon-isotope cycles. Palaeogeogr. Palaeoclimatol. Palaeoecol. 577, 110562.

Ruebsam, W., Mayer, B., and Schwark, L., 2019. Cryosphere carbon dynamics control early Toarcian global warming and sea level evolution. Global and Planetary Change. 172, 440-453.

Ruebsam, W., Thibault, N., and Al-Husseini, M.I, 2020. Chapter 12 - early Toarcian glacioeustatic unconformities and chemostratigraphic black holes. In: Montenari, M. (Ed.), Stratigraphy and Timescales 5, Carbon Isotope Stratigraphy. https://doi.org/ 10.1016/bs.sats.2020.08.006.

Ruhl, M., Hesselbo, S.P., Hinnov, L., Jenkyns, H.C., Xu, W., Storm, M., et al., 2016. Astronomical constraints on the duration of the Early Jurassic Pliensbachian Stage and global climatic fluctuations. Earth Planet. Sci. Lett. 455, 149–165.

Scotese, C., 2023. Toarcian, PALEOMAP PaleoAtlas, School of Geosciences, The University of Sydney, Australia. https://www.earthbyte.org/paleomap-paleoatlas-for-gplates/

Sharland, P.R., Archer, R., Casey, D.M., Davies, R.B., Hall, S.H., Heward, A.P., Horbury, A.D., and Simmons, M.D. (2001). Arabian Plate Sequence Stratigraphy. GeoArabia Special Publication 2, Gulf PetroLink, Bahrain, 371 p., with 3 charts.

Stewart, S.A., Reid, C.T., Hooker, N.P. and Kharouf, O.W., 2016, Mesozoic siliciclastic reservoirs and petroleum system in the Rub' Al-Khali basin, Saudi Arabia: AAPG Bulletin, v. 100, no. 5, p. 819–841.

Storm, M.S., Hesselbo, S.P., Jenkyns, H.C., Ruhl, M., Ullmann, C.V., Xu, W., et al. 2020. Orbital pacing and secular evolution of the Early Jurassic carbon cycle. Proc. Natl. Acad. Sci. 117, 3974–3982.

van de Schootbrugge, B., Richoz, S., Pross, J., Luppold, F.W., Hunze, S., Wonik, T., Blau, T., Meister, C., van der Weijst, C.M.H., Suan, G., Fraguas, A., Fiebig, J., Herrle, J.O., Guex, J., Little, C.T.S., Wignall, P.B., Püttmann, W., Oschmann, W., 2018. The Schandelah Scientific Drilling Project: a 25-million year record of Early Jurassic palaeo-environmental change from northern Germany. Newsl. Stratigr. 52 (3), 249–296.

Xu, W., Ruhl, M., Jenkyns, H.C., Leng, M.J., Huggett, J.M., Minisini, D., Ullmann, C.V., Riding, J.B., Weijers, J.W.H., Storm, M.S., Percival, L.M.E., Tosca, N.J., Idiz, E.F., Tegelaar, E.W., Hesselbo, S.P., 2018. Evolution of the Toarcian (Early Jurassic) carbon cycle and global climatic controls on local sedimentary processes (Cardigan Bay Basin, UK). Earth Planet. Sci. Lett. 484, 396–411.

Figure 1: Paleogeogeographic reconstruction of the Toarcian (183.7 to 174 Ma) indicates the Arabian Plate straddled the Equator along the southern margin of the Neo-Tethys Ocean (Scotese, 2023). Localities in the article: (1) Central Saudi Arabia, (2) Kuwait, (3) Wadi Sahtan in Oman. (4) Chacay Melehue in Argentina, (5) Hispanic Corridor, (6) Penniche in Portugal, and (7) Mochras borehole in UK.

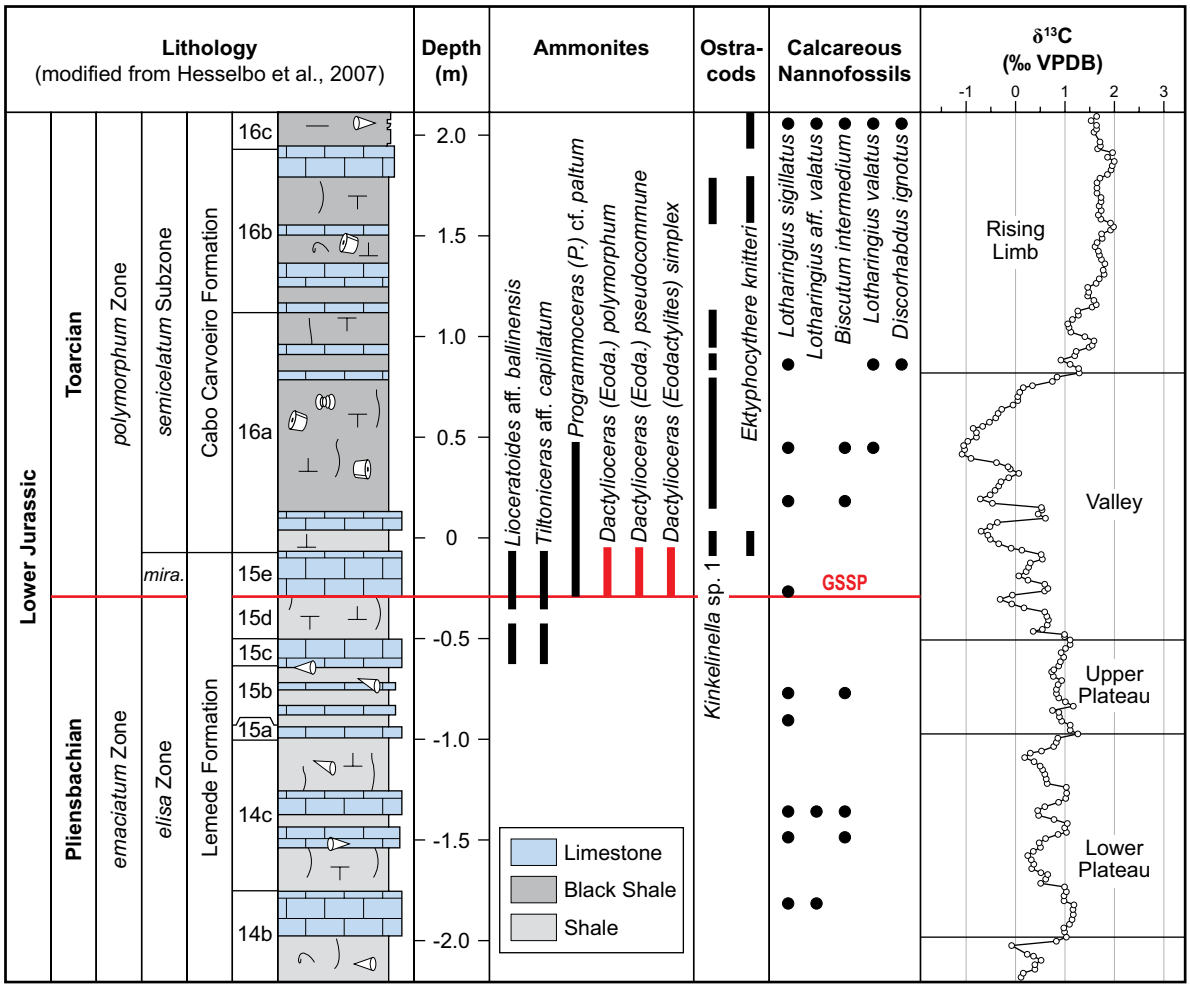

Figure 2: The Global Stratotype Section and Point (GSSP) of the base Toarcian Stage is defined in the Penniche section in Portugal by the first occurrence (FO) of the ammonite *Dictylioceras polymorphum* (Fucini) (Bordalo da Rocha et al., 2016; Hesselbo et al., 2020). The stage boundary occurs in the Pliensbachian-Toarcian carbon-isotope excursion (Pl-T-CIE) in a carbon-13 isotope ($\delta^{13}C$) negative valley above a $\delta^{13}C$ plateau and below a $\delta^{13}C$ rising limb.

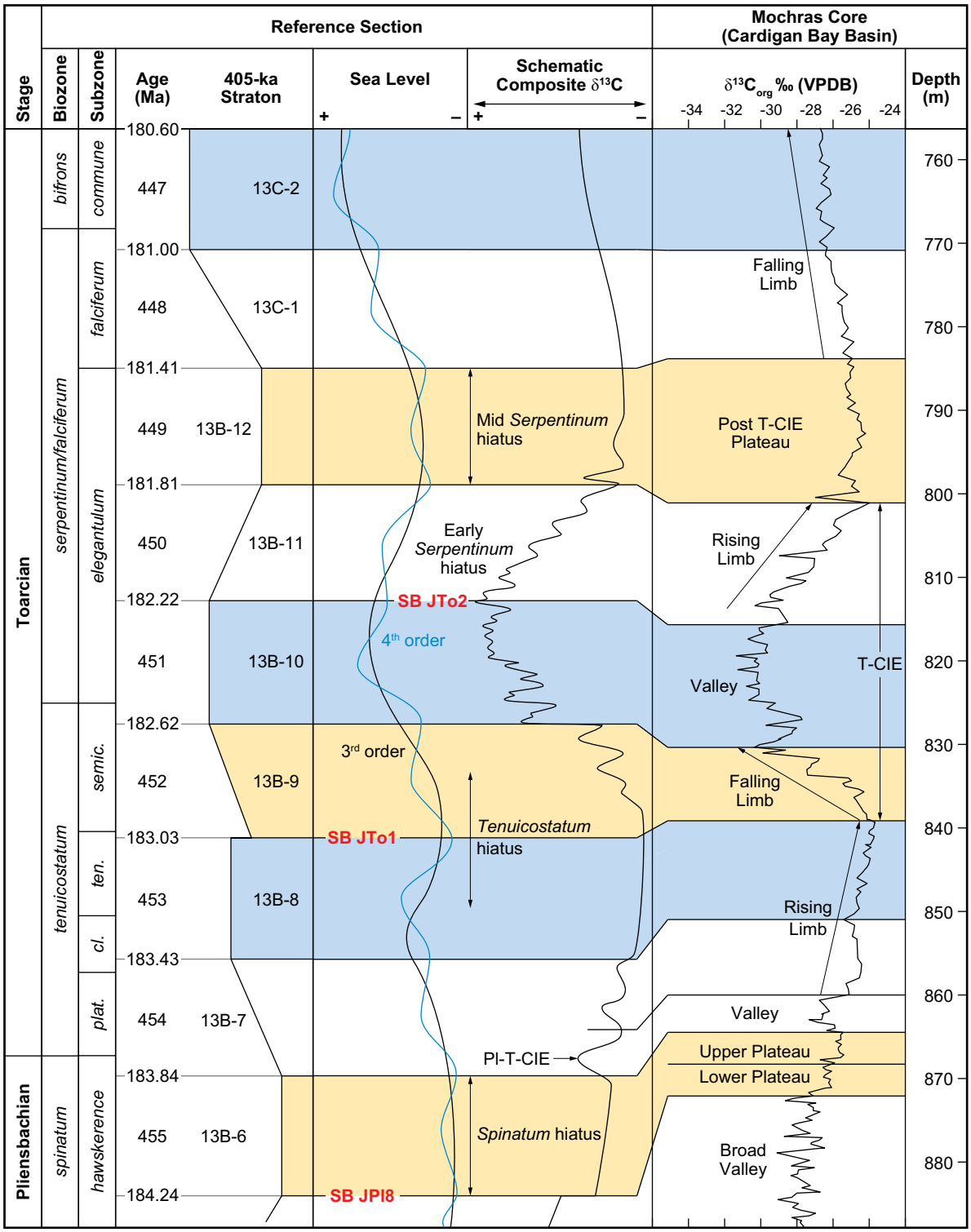

Figure 3: Uppermost Pliensbachian and Lower Toarcian $\delta^{13}C$ reference curve and the $\delta^{13}C_{org}$ record in the Mochras borehole (Storm et al., 2020 and references therein), with glacio-eustatic interpretation calibrated with c. 405 ka stratons (Ruebsam and Al-Husseini, 2020, 2021).

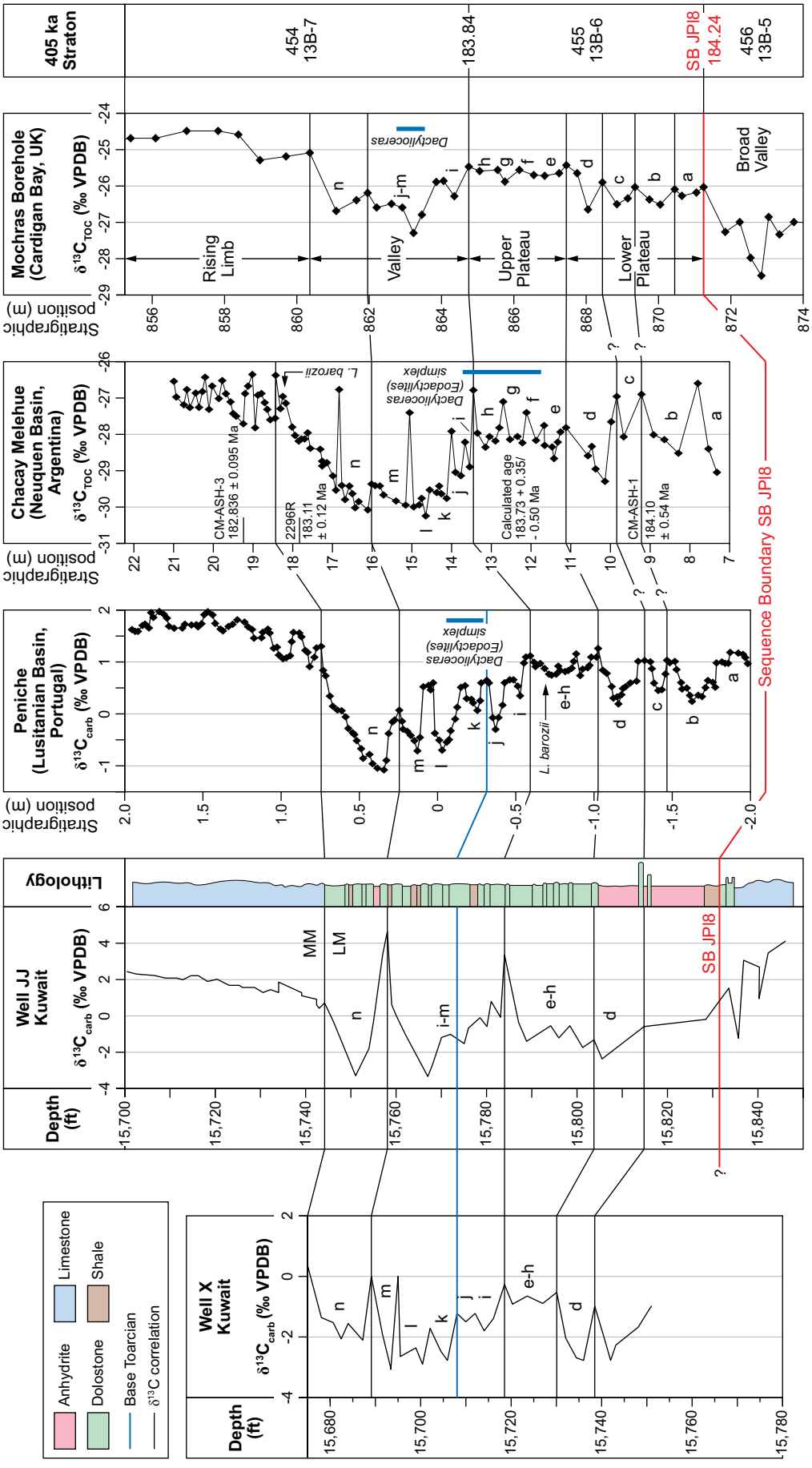

Figure 4: Correlation of carbon-13 isotope ($\delta^{13}C$) records spanning the base Toarcian Stage defined in the GSSP in the Penniche section in Portugal (Fig. 2, Bordalo da Rocha et al., 2016; Hesselbo et al., 2020). The GSSP occurs in the lower part of the distinct $\delta^{13}C$ valley evident in boreholes JJ and X (De Keyser et al., in review), Mochras borehole (Storm et al., 2020 and references therein); and Chacay Melehue (Al-Suwaidi et al., 2022). Uppermost Pliensbachian global sequence boundary SB JPl8 is positioned at the base of the lower $\delta^{13}C$ plateau in the Mochras borehole (Ruebsam and Al-Husseini, 2021), and is correlated to an unconformity below massive anhydrites in borehole JJ in Kuwait (De Keyser et al., in review). Biostratigraphic interpretations in Kuwait indicate the Pliensbachian-Toarcian transition spans the boundary between the Lower and Middle Marrat members (LM/MM) in borehole JJ (Crespo de Cabrera et al., 2023).

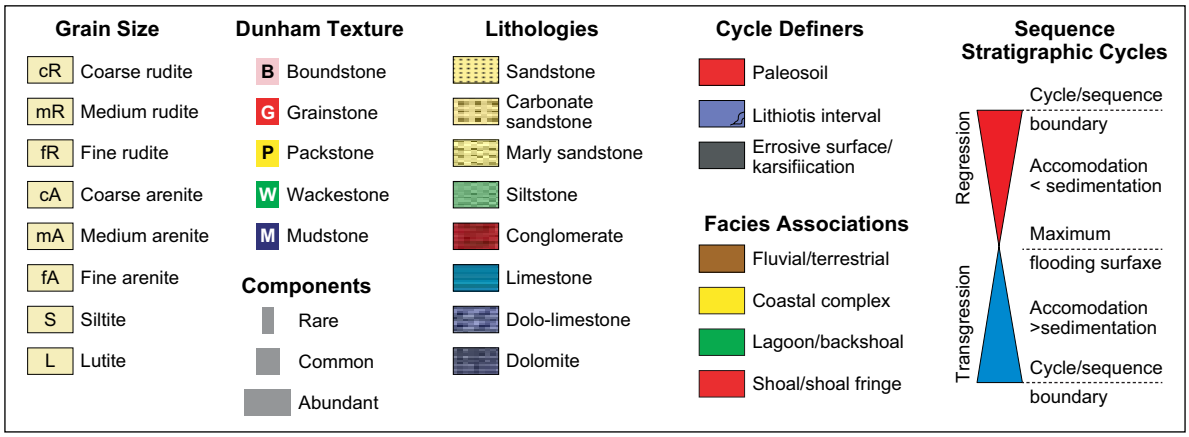

Figure 5: (a) Description and **(b)** sequence architecture of the type section of the Mafraq Formation in Wadi Sahtan in Oman (Bendias and Aigner, 2015. See Fig. 1 for location. The lower part of the negative Toarcian carbon-isotope excursion (T-CIE) occurs above the Lithiotis Limestone and below the pre-Dhruma unconformity, corresponding to a hiatus that spans most of the Toarcian and Aalenian. The base Toarcian Stage (183.7 Ma) and uppermost Pliensbachian global sequence boundary SB JPl8 (184.2 Ma) are positioned in the lower part of the $\delta^{13}C$ valley and at the base of $\delta^{13}C$ plateau in the Pliensbachian-Toarcian CIE. Cycle sets CS-1 to CS-23 are likely tuned by the c. 100 ka short-eccentricity e-cycle.

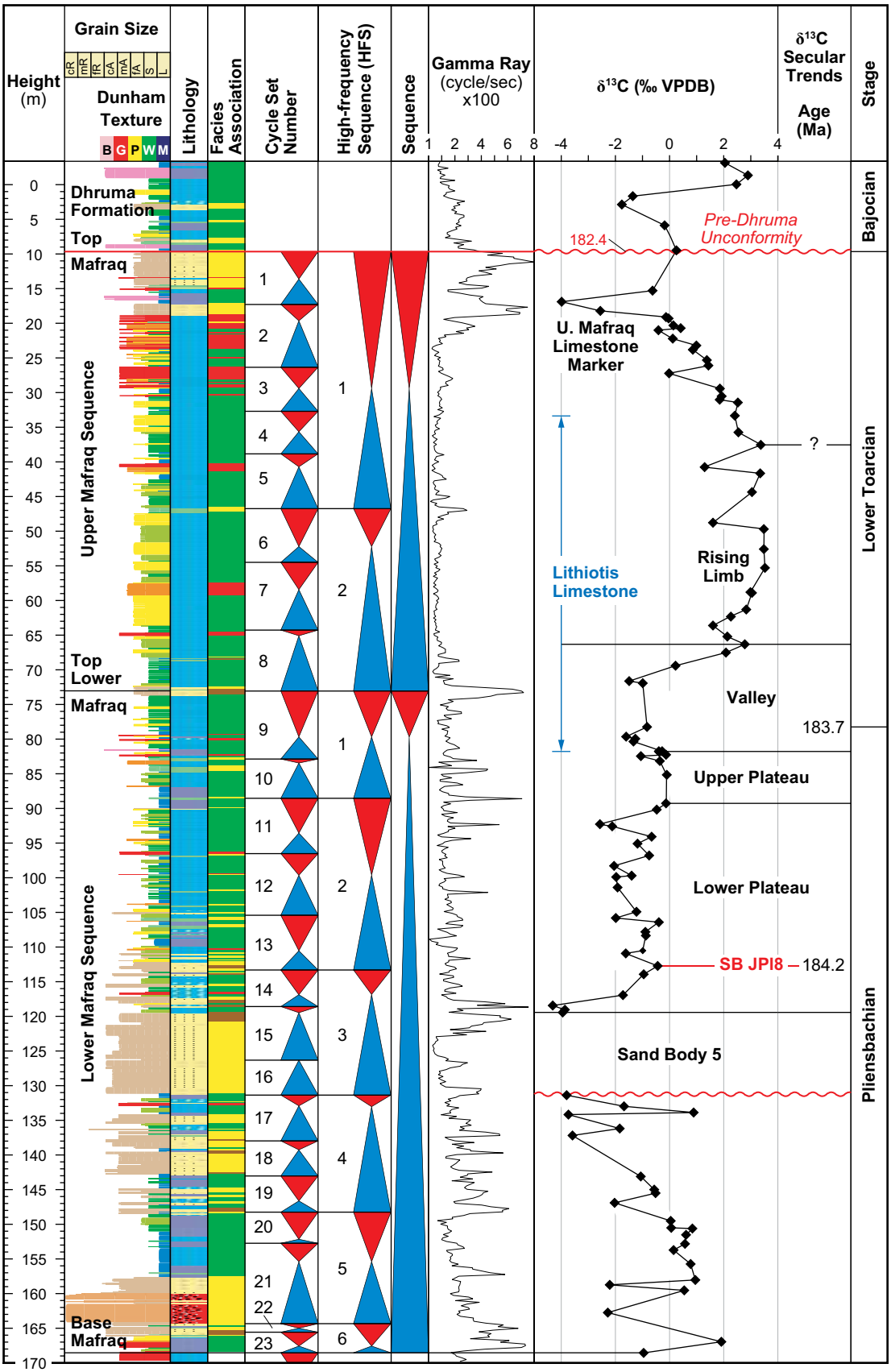

Figure 5b: *(See figure 5a for caption).*

Supplementary Information

Calibrating the Pliensbachian-Toarcian transition in Arabia

Moujahed Al-Husseini

Previously Aramco, Saudi Arabia, and GeoArabia, Bahrain
moujaheda@gmail.com

1. Abbreviations for age and duration

Following the recommendations of the International Union of Geological Sciences (IUGS) and the International Union of Pure and Applied Chemistry (IUPAC) both durations and ages in thousands of years are abbreviated as 'ka' for *kilo annus*; and in millions of years as 'Ma' for *Mega annus* (Holden et al., 2011).

2. Global Stratotype Section and Point (GSSP) for the base Toarcian Stage

The GSSP (i.e., 'Golden Spike') for the base Toarcian Stage is defined in the Penniche section in Portugal (Fig. 1) (Bordalo da Rocha et al., 2016). This GSSP was formally approved by the International Commission on Stratigraphy (ICS) of the International Union of Geological Sciences (IUGS) and is summarized in the publication 'Geological Time Scale 2020' – GTS 2020 (Fig. 1., after Hesselbo et al., 2020, in Gradstein et al., 2020).

In the Penniche section the base Toarcian Stage is defined by the first occurrence (FO) of the ammonite *Dictylioceras polymorphum* (Fucini) (Fig. 1), which is assumed to be equivalent in other sections to the FO of ammonites *Dactylioceras (Eodactylites)* cf. simplex (Fucini) and *Dactylioceras tenuicostatum* (Young & Bird) (Page, 2004; Macchioni, 2002). In biostratigraphically complete sections that span the stage boundary the first occurrences of these ammonites occur in the Pliensbachian-Toarcian carbon-isotope excursion (Pl-T-CIE) (Fig. 1; Hesselbo et al., 2007; Littler et al., 2010; Ruebsam and Al-Husseini, 2020; Ruebsam et al., 2020). In the present study, the Pl-T-CIE in the Penniche GSSP is characterized by carbon-isotope ($\delta^{13}C$) secular patterns consisting from base-up of a Pliensbachian broad valley, lower and upper plateaus, a valley containing the base Toarcian Stage in its lower part, and a Toarcian rising limb (Fig. 1).

3. Stratigraphic positions of ammonite zonal boundaries in the Mochras borehole

In the Mochras borehole Al-Suwaidi et al. (2022, their figure 4) showed the accurate stratigraphic position of the stage boundary at 863 m in the $\delta^{13}C$ valley; however, in their figure 5 (reproduced in Fig. S1), the stage boundary is shown in the $\delta^{13}C$ plateau corresponding to 866 m. Also, in the Mochras borehole, Al-Suwaidi et al. (2022) shifted the position of the Tenuicostatum-Serpentinum zonal boundary by 9 m, from 831 m in their figure 4 to 840 m in their figure 5. These shifts result in incorrect age calibrations of the ammonite zonal boundaries and $\delta^{13}C$ secular intervals in the Mochras borehole.

4. Astronomical Time Scale (ATS) and the 405-ka Metronome

The Earth's long-term orbit around the Sun is elliptical and represented by the sum of Fourier sinusoidal components, of which the 405,000-year component has the greatest amplitude (Laskar et al., 2004). The 405-ka elliptical resonance of the Earth's orbit is caused by the gravitational 'tug-of-war' between Venus (planet 2) and Jupiter (planet 5), and is referred to as the g2-g5 metronome (Fig. S2, Laskar et al., 2004), or the 'tuning fork' (Matthews and Frohlich, 2002), and is commonly extracted by spectral analysis of rhythmic stratigraphic records using cyclostratigraphy (e.g., Huang, 2018). The 405-ka cycle is predicted to have a uniform period to 250 Ma (Laskar et al., 2004), as has been verified in several studies (e.g., Kent et al., 2018), and even as far back as 1.5 billion years ago in Australia (Lantink et al., 2019).

In the Geologic Time Scale GTS 2020 the intervals between the eccentricity minima of the 405-ka metronome are referred to as astrochronozones (ACZ, Fig. S2) and are used to calibrate biozones and magnetic chrons in the Neogene (2.58–23.04 Ma) (Raffi et al., 2020), and references therein). The cycles in the 405-ka metronome are prefixed by 'E' (Hinnov, 2018; Huang, 2018) with the first eccentricity maximum value in E1 at 192.125 ka (Fig. S2). Calculating the eccentricity maximum for the Nth cycle EN is given by the arithmetical formula: Maximum EN = 0.192125 + (N-1) x 0.405 Ma.

Huang (2018) adopted the estimate for the base Toarcian Stage at 183.7 Ma (Ogg et al., 2016) at the maximum eccentricity value of E454 in the 405-ka metronome of ATS 2018. Using the metronome formula, the maximum value of E454 has an age of 183.657125 Ma, rounded-off to c. 183.7 Ma.

5. Orbital scale of glacio-eustasy and time scale

The orbital scale of glacio-eustasy is based on a simplified model of orbital-forcing of insolation (Matthews and Frohlich, 2002; Matthews and Al-Husseini, 2010). It consists of 'dozons', each formed by 12 chronostratigraphic units named 'stratons' (Fig. S2). Stratons are tuned by the long-eccentricity 405-ka cycle and dozons have a duration of 4.86 Ma. Three dozons (A, B and C in ascending order) form a 14.58-Ma 'orbiton', which are numbered in descending order with Orbiton 1 starting at SB1 at 16.166 Ma and ending at SB0 at 1.586 Ma. Stratons are numbered from 1 to 12 in every dozon in ascending order and the scale predicts stratons 6, 9 and 12 in any dozon are unconformity-prone sea-level lowstands, and stratons 2, 8 and 10 are sea-level highstands. In this scale sequence boundaries (SB) occur at eccentricity minima between stratons.

Stratons are also numbered as integers relative to present time starting with base Straton 1 at 0.371 ka (Fig. S2), and base Straton N at 0.371 + (N-1) x 0.405 Ma (Matthews and Al-Husseini, 2010). The age at the base of any 405-ka straton differs from the minima of the 405-metronome by 23,625 years (Hinnov, 2018). This difference occurs because base Straton 1 starts at the minimum of total eccentricity at 371,000 years before present rather than the minimum of the 405-ka metronome at 394,625 years before present (Fig. S2).

In the ATS the base Toarcian at 183.7 Ma occurs in the maximum eccentricity value of E454 at 183.657125 Ma (rounded-off to 183.7 Ma). In the orbital scale the start/base of Straton 454 = 0.371 + (453) x 0.405 Ma = 183.836 Ma The maximum eccentricity in Straton 454 occurs 0.2025 Ma after its start at 183.6335 Ma compared to 183.657125 Ma, a difference of 23,625 years.

6. Eccentricity-forcing of glacio-eustasy

The estimated duration of fourth-order Mesozoic and Paleozoic sequences is c. 400 ka (Haq, 2014; Haq, 2018, Haq and Schutter, 2008). Based on the simplified model of orbital-forcing of glacio-eustasy Matthews and Frohlich (2002) concluded fourth-order sequences (stratons) are tuned by the 405-ka long-eccentricity cycle and the much longer c. 2.4 Ma eccentricity cycle tunes third-order T-R sequences at 2.4 ± 0.4 Ma (mainly 2.0 and 2.8 Ma). Matthews and Frohlich (2002) considered obliquity (c. 40 ka) and precession (c. 20 ka) to be higher-frequency cycles that are mainly significant during intra-glacial intervals. This conclusion can be seen by examining the glacio-eustatic cycles in the past 800 ka (Fig. S3).

During the past 800 ka glacio-eustatic cycles with amplitudes reaching c. 125 m are numbered starting with present-day interglacial numbered 1 (Al-Husseini, 2013 and references therein). The start of post-glacial sea-level rises (i.e., glacial terminations or glacial maxima) correspond to even-numbered sequence boundaries (SB) and their ages are approximately estimated in several studies (e.g., Miller, 2005; Al-Husseini, 2013, and references therein). A visual examination of the glacio-eustatic pattern indicates they mainly track the short-eccentricity cycles (c. 100 ka) and to a lesser extent the obliquity (c. 40 ka) cycles, with little if any evidence of the precession cycles (c. 20 ka). In high-resolution sequence stratigraphy the c. 100 and 40 ka cycles form fifth- and sixth-order sequences.

The dominance of the c. 100-ka glacio-eustatic cycles suggests the 405-ka cycle is not a significant driver of glacio-eustasy. Although the visual evidence for the 405-ka cycle may be subtle, its significance becomes clear by examining the glacio-eustatic signal in the interval between interglacials 13a and 9e (Fig. S3). In this interval eccentricity cycle e5 attains minimum values of c. .01 at 371 and 435 ka, and a maximum of only 0.02 at c. 400 ka, and obliquity cycles k and m are not evident in the sea-level curve. This pattern indicates interglacial 11c was bounded by more extreme cold climates when the Earth's orbit was nearly circular (low eccentricity).

During times when eccentricity was greater than 0.02 the orbit was more eccentrical, climate was warmer and the obliquity cycles are evident in the interglacial intervals. This pattern is particularly evident in e3 when eccentricity exceeded 0.05 and obliquity cycles g and h are expressed in interglacial 7. Much higher-frequency, low-amplitude fluctuations in interglacial 7 may represent precession cycles. A similar pattern to interglacial 7 occurs in interglacial 15 when eccentricity cycle e7 also exceeded 0.05. In this interglacial the signal between obliquity cycles p and q is expressed as interglacial peaks 15a and 15c, separated by glaciation 15b.

The pattern between eccentricity, obliquity and glacio-eustasy in the 800-ka interval leads to a simple insight: the more circular the Earth's orbit (low eccentricity) the more likely ice sheets will expand, and *vice versa.* This pattern can be extrapolated to older times implying the c. 405-ka eccentricity cycle drives the fourth-order glacio-eustatic signal, and obliquity and to a much lesser extent precession interfere with the signal during interglacial intervals. This insight provides an approximate formula for dating 405-ka stratons corresponding to glacio-eustatic lowstands based on the orbital scale and the metronome.

For example, the scale predicts the starts of Stratons 1 and 2 at 371 and 776 ka, and the metronome minima of E1 and E2 occur at 394.625 and 799.625 ka. These ages are approximate estimates for SB 10 at c. 340 ka marking the start of the de-glaciation 5e (Termination IV), and SB 20 at c. 795 ka. These age comparisons indicate the orbital and metronome estimates match the ages for SB 10 and SB 20 with an accuracy of ± 30–50 ka. Such uncertainties for dating surfaces in deep time are considered comparable to high-precision radiometric estimates which are the order ± 100 ka at best.

7. Dating SB JPl8

Straton 455 occurs between c. 184.24 and 183.84 Ma and corresponds in the orbital Scale to c. 405-ka Straton 6 in 4.86-Ma Dozon B of 14.58-Ma Orbiton 13, denoted 13B-6 (Matthews and Al-Husseini, 2010; Ruebsam and Al-Husseini, 2021). As the sixth straton of Dozon 13B it is predicted as a low glacio-eustatic sea level and an unconformity-prone unit. The sequence boundary marking the maximum sea level fall (maximum regression surface, MRS) and the start of the overlying transgression is placed at the base/start of 13B-6 at 184.24 Ma and correlated to SB JPl8 estimated at 184.3 Ma (Haq, 2018).

Acknowledgements

The author thanks Arnold Egdane for designing the manuscript.

References

Al-Husseini. M.I., 2013. Antarctica's glacio-eustatic signature in the Aptian and late Miocene–Holocene: Implications for what drives sequence stratigraphy. *GeoArabia,* v. 18, no. 1, p. 17-52.

Al-Suwaidi, A., Ruhl, M., Jenkyns, H. C., et al, 2022. New age constraints on the Lower Jurassic Pliensbachian-Toarcian boundary at Chacay Melehue (Neuquen Basin). Argentina. Scientific Reports 12, 4975.

Boralo da Rocha, R., Mattioli, E. Duarte, L.V., Pittet, B., lmi, S., Mouterde, R., Cabral, M.C., Comas-Rengifo, M.J., Gómez, J.J.,, Goy, A., Hesselbo, S.P., . Jenkyns. H.C.., Littler. K., Mailliot, S., Veiga de Oliveira. L.C., Osete M.L., Perilli, N., Pinto, S., Ruget, C. and G Suan, G., 2016. Base of the Toarcian Stage of the Lower Jurassic defined by the Global Boundary Stratotype Section and Point (GSSP) at the Peniche section (Portugal). Episodes Vol. 39, no. 3, 460-481.

Gradstein, F.M., Ogg, J.G., Schmitz, M.D., Ogg, G.M. (Eds.), Geologic Time Scale 2020, Elsevier Inc.

Haq, B.U., 2014, Cretaceous eustasy revisited. Global and Planetary Change, 113, 44-58.

Haq, B.U., 2018. Jurassic sea level variations: a reappraisal. Geol. Soc. America, GSA Today, 1, soi: 10.1130/GSATG359A.1

Haq, B.U. and Schutter, S.R. 2008. A chronology of Paleozoic sea-level changes. Science 322, 6s-68.

Hesselbo, S.P., Jenkyns, H.C., Duarte, L.V., abd Oliveira, L.C.V., 2007. Carbon-isotope record of the early Jurassic (Toarcian) Oceanic Anoxic Event from fossil wood and marine carbonate (Lusitanian Basin, Portugal). Earth Planet. Sci. Lett. 253, 455–470.

Hesselbo, S.P., Ogg, J.G., Ruhl, M., Hinnov, C., and Huang, C., 2020. Chapter 26, The Jurassic Period. In Gradstein, F.M., Ogg, J.G., Schmitz, M.D., Ogg, G.M. (Eds.), Geologic Time Scale 2020, v. 2, 965–1021. Elsevier Inc.

Hinnov, L., 2018. Cyclostratigraphy and Astrochronology in 2018 In: Montenari, M. (Ed.), Stratigraphy and Timescales. vol. 3. 1–80. Elsevier Inc.

Holden, N.E., Bonardi, M.L., De Bièvre, P., Renne, P.R., Villa, I.M., 2011. IUPAC-IUGS common definition and convention on the use of the year as a derived unit of time (IUPAC Recommendations 2011). Pure and Applied Chemistry 83 (5), 1159-1162. https://doi.org/10.1351/PAC-REC-09-01-22.

Huang, C., 2018. Astronomical time scale for the Mesozoic. In: Montenari, M. (Ed.), Stratigraphy and Timescales. vol. 3. p. 81–150. Elsevier Inc,

Kent, D.V., Olsen, P.E., Rasmussen, C., Lepre, C., Mundil, R., Irmis R.B., Gehrels, G.E. Giesler, D., Geissman J.W. and Parker, W.G., 2018. Empirical evidence for stability of the 405-kiloyear Jupiter–Venus eccentricity cycle over hundreds of millions of years. PNAS, vol. 115 | no. 24 | 6153–6158.

Lantink M.L, Davies J.H.F.L, Mason P.R.D., Schaltegger U., and Hilgen F.J., 2019, Climate control on banded iron formations linked to orbital eccentricity. Nat Geosci. 12(5):369-374.

Laskar, J., Robutel, P., Joutel, F., Gastineau, M., Correia, A.C.M., and Levrard, B. (2004). A long-term numerical solution for the insolution quantities of the Earth. Astron. Astrophys. 428, 261–285.

Macchioni, F., 2002. Myths and legends in the correlation between the Boreal and Tethys. Implications on the dating of the Oceanic Anoxic Event in Lower Toarcian age OAE and on the mass extinction of the Lower Toarcian: Geobios, Mémoire Spécial 35, p. 150–164.

Matthews, R.K., and Frohlich, C., 2002. Maximum flooding surface and sequence boundaries: Comparisons between observation and orbital forcing in the Cretaceous and Jurassic (65-190 Ma). GeoArabia 7(3), 503–538.

Matthews, R.K., and Al-Husseini, M.I., 2010. Orbital-forcing glacio-eustasy: a sequence-stratigraphic time scale. GeoArabia 15 (3), 155–167.

Miller, K.G., Kominz, M.A., Browning, J.V., Wright, J.D., Mountain, G.S., Katz, M.E., Sugarman, P.J., Cramer, B.S., Christie-Blick N., and Parker, S.F., 2005. The Phanerozoic record of global sea-level change. Science, 310, p. 1293-1298.

Ogg, J., Ogg, G., and Gradstein, F., 2016. A Concise Geologic TimeScale 2016. Elsevier Inc.

Page, K.N.A. Sequence of biohorizons for the subboreal province Lower Toarcian in Northern Britain and their correlation with a submediterranean standard. Riv. Ital. Paleontol. Stratigr. 110, 109–114 (2004).

Raffi, I., Wade, B.S. and Palike, H. (with contributions by A.G. Beu, R. Cooper, M.P. Crundwell, W. Krijgsman, T. Moore, I. Raine, R. Sardella and Y.V. Vernyhorova, 2020. Chapter 29. The Neogene Period. In Gradstein, F.M., Ogg, J.G., Schmitz, M.D., Ogg, G.M. (Eds.), Geologic Time Scale 2020, v. 2, 1141-1215. Elsevier Inc.

Ruebsam, W. and Al-Husseini, M.I, 2020. Calibrating the Early Toarcian (Early Jurassic) with stratigraphic black holes (SBH). Gondwana Research 82, 317–336.

Ruebsam, W. and Al-Husseini, M.I., 2021. Orbitally synchronized late Pliensbachian– early Toarcian glacio-eustatic and carbon-isotope cycles. Palaeogeogr. Palaeoclimatol. Palaeoecol. 577, 110562.

Ruebsam, W., Thibault, N., Al-Husseini, M.I, 2020. Chapter 12 - early Toarcian glacioeustatic unconformities and chemostratigraphic black holes. In: Montenari, M. (Ed.), Stratigraphy and Timescales 5, Carbon Isotope Stratigraphy. https://doi.org/ 10.1016/bs.sats.2020.08.006.

Storm, M.S., Hesselbo, S.P., Jenkyns, H.C., Ruhl, M., Ullmann, C.V., Xu, W., et al. 2020. Orbital pacing and secular evolution of the Early Jurassic carbon cycle. Proc. Natl. Acad. Sci. 117, 3974–3982.

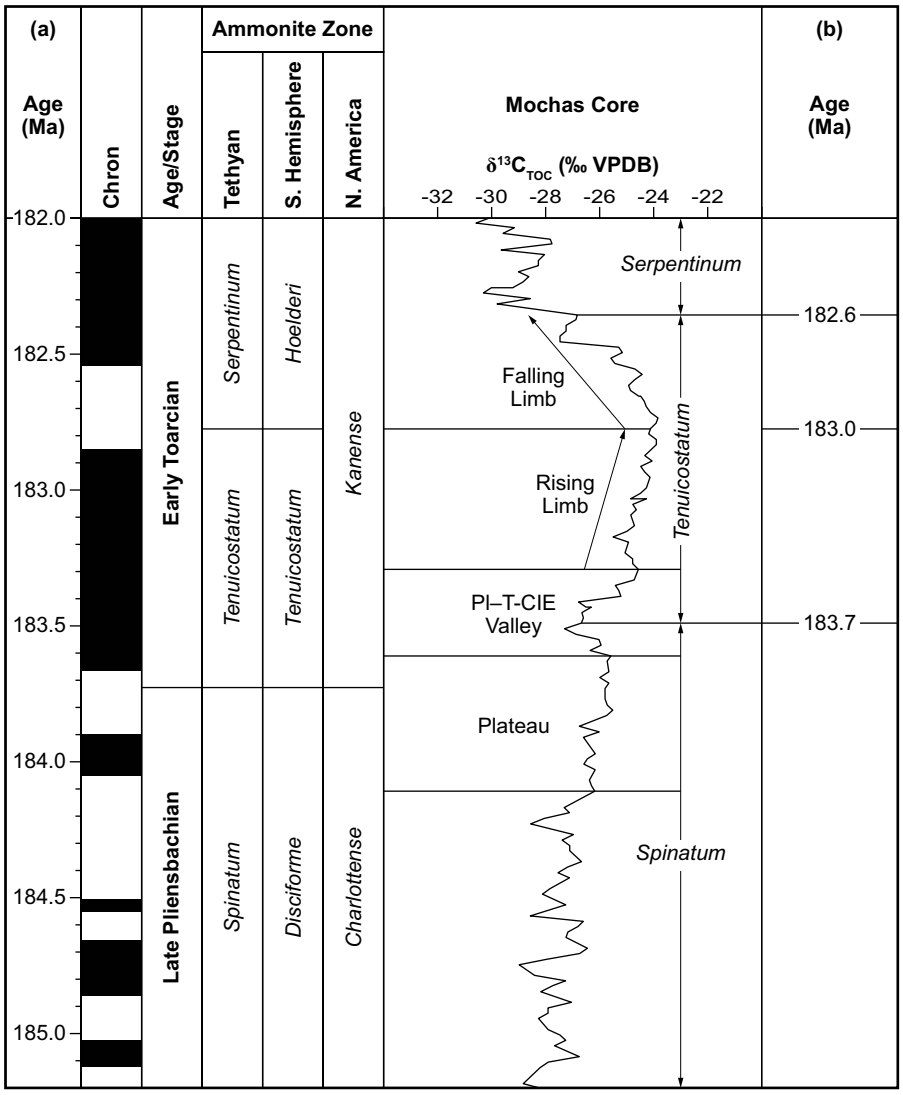

Figure S1: (a) In the age model of the Mochras borehole Al-Suwaidi et al. (2022) shifted the position of the base Toarcian Stage in the Pl-T-CIE from within the $\delta^{13}C$ valley (their figure 4) to the upper plateau (their figure 5, reproduced in Fig. S1). Also, Al-Suwaidi et al. (2022) shifted the position of the Tenuicostatum-Serpentinum zonal boundary from the top of the $\delta^{13}C$ falling limb of the T-CIE (their figure 4) to its base (their figure 5). **(b)** The boundaries of ammonite zones and $\delta^{13}C$ secular intervals in the Mochras borehole are picked to an accuracy of better than 1.0 meter (Storm et al., 2020, and references therein), and their calibrations represent the age model of the late Pliensbachian and Early Toarcian reference section (Fig. 3, Table S1, Ruebsam and Al-Husseini, 2020, 2021).

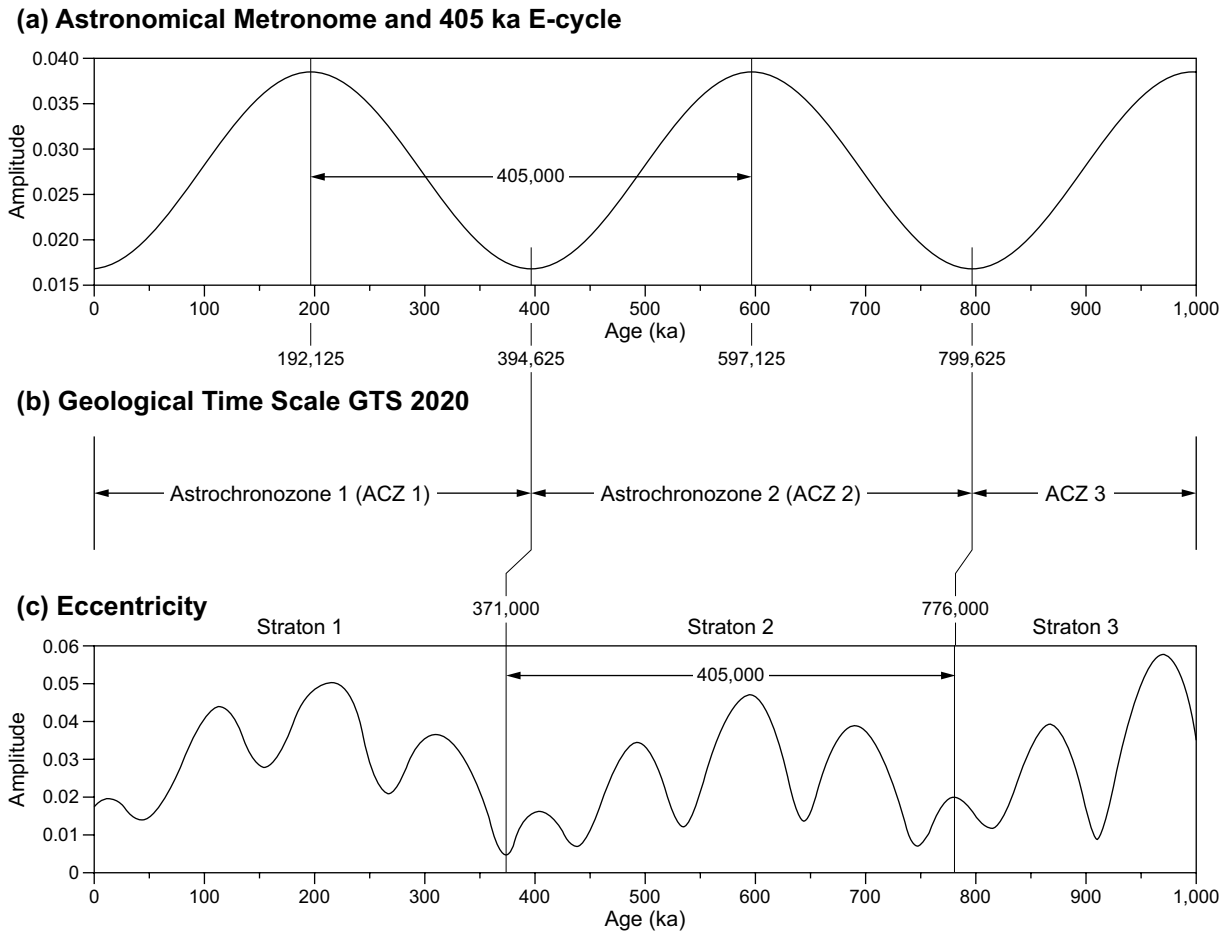

Figure S2: (a) The 'Astronomical Metronome' corresponds to the leading sinusoidal component of the Earth's eccentrical orbit around the Sun, which has a period of 405,000 years (405 ka). **(b)** In the 'Geological Time Scale 2020' (GTS 2020, Raffi et al., 2020, in Gradstein et al., 2020) biozones and magnetic reversals in the Neogene Period (2.59–23.04 Ma) are calibrated with 405-ka astrochronozones (ACZ) that are numbered as integers between the minima of the metronome. **(c)** In the orbital scale of glacio-eustasy c. 405-ka time-rock units (stratons) also occur approximately between the minima of eccentricity (Matthews and Frohlich, 2002).

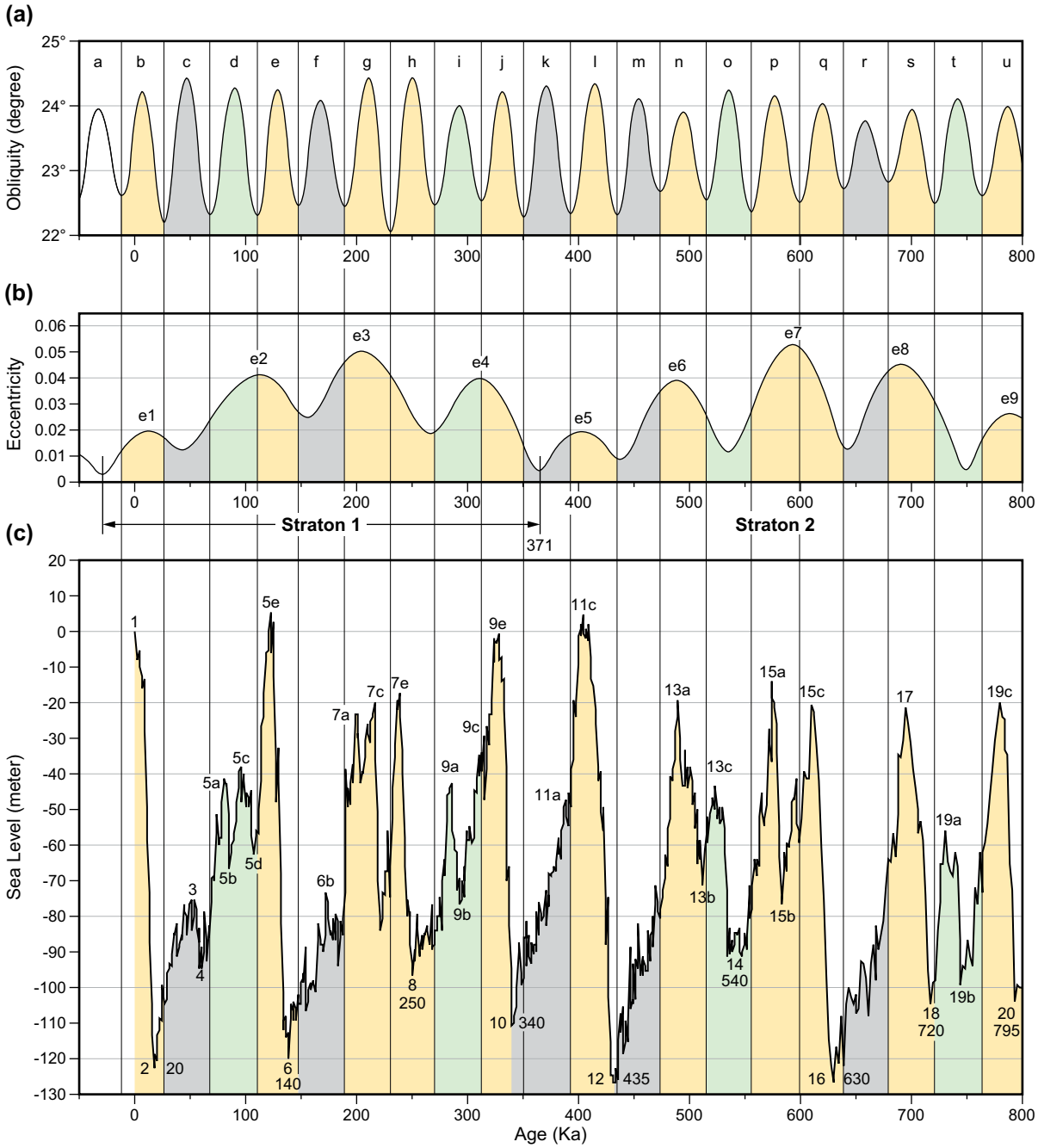

Figure S3: Correlation of obliquity **(a)**, eccentricity **(b)** and sea level **(c)** cycles during the past 800 ka (Miller, 2005; see 'Milankovitch Cycles' in Wikipedia) indicates more circular Earth orbits (low eccentricity) correlate to colder climates and glaciations. During the most circular orbits at c. 370 and 435 ka bounding eccentricity cycle e5, grey obliquity cycles k and m are not expressed in the sea level cycle during Glaciations 10 and 12. In contrast, yellow obliquity cycles are expressed in the sea-level curve during eccentricity high values and interglacial intervals. Green obliquity cycles are expressed in the sea-level curve during changes in high eccentricity cycles coinciding with obliquity cycles. High-frequency sea-level cycles of the order of 5–20 m may be driven by precession cycles.

Table S1: Age model of Mochras Borehole (Ruebsam and Al-Husseini, 2020, 2021)

Position	Depth (meter)	Age (Ma)
Base Bifrons	768	180.9
Base Falling Limb = Top post-T-CIE Plateau	783	181.4
Base post-T-CIE Plateau = Top T-CIE Rising Limb	801	181.8
Top T-CIE Valley	815	182.2
Base T-CIE Valley = Tenuicostatum/serpentinum	830	182.6
Base T-CIE Falling Limb = Top post- PI-T-CIE Rising Limb	839	183.0
Base post- PI-T-CIE Rising Limb = Top PI-T-CIE Valley	860.5	
Spinatum/tenuicostatum	863	183.7
Base PI-T-CIE Valley	864.8	183.84
Base Lower Plateau = SB JPl8	871.0	184.24
Margaritatus/spinatum	901	185.3